Applied Surface Science 579 (2022) 152188

Contents lists available at ScienceDirect

Applied Surface Science

journal homepage: www.elsevier.com/locate/apsusc

Full Length Article

Comparative study on the nanomechanical behavior and physical properties influenced by the epitaxial growth mechanisms of GaN thin films

Najla Boughrara [a], Zohra Benzarti [a,*], Ali Khalfallah [b,c,d], Manuel Evaristo [b], Albano Cavaleiro [b]

[a] Laboratory of Multifunctional Materials and Applications (LaMMA), Department of Physics, Faculty of Sciences of Sfax, University of Sfax, Soukra Road km 3.5, B.P. 1171, Sfax 3000, Tunisia
[b] CEMMPRE, Department of Mechanical Engineering, University of Coimbra, Rua Luís Reis Santos, Coimbra 3030-788, Portugal
[c] Laboratoire de Genie Mécanique, Ecole Nationale d'Ingénieurs de Monastir, University of Monastir, Av Ibn El-Jazzar, Monastir 5019, Tunisia
[d] DGM, Institut Supérieur des Sciences Appliquées et de Technologie de Sousse, University of Sousse, Cité Ibn khaldoun, Sousse 4003, Tunisia

ARTICLE INFO

Keywords:
GaN
Carrier gas
Epitaxial growth mode
Dislocation density
Nanoindentation
Loading rate

ABSTRACT

The effect of carrier gas on nanomechanical properties of GaN thin films grown on (0001) sapphire substrates by metal–organic chemical vapor deposition (MOCVD) process, was studied by Berkovich nanoindentation. GaN/H_2 and GaN/N_2 films were deposited using hydrogen and nitrogen, as carrier gases, respectively. New method was developed to compute the contact stiffness versus the penetration depth using a single load–displacement curve. It was found that the hardness and Young's modulus of GaN/H_2 are lower than those of GaN/N_2. Moreover, pop-in events were revealed for GaN/H_2, in contrast for GaN/N_2. Fracture was only manifested in the imprint of GaN/N_2 due to its low fracture toughness. Besides, it was disclosed the high sensitivity of loading rate only for GaN/H_2. The GaN/N_2 sample experiences plastic strain relaxation, while GaN/H_2 is a highly stressed sample; hence, it has less dislocation density compared to GaN/N_2 sample. We demonstrated that the used carrier gas influences on GaN epitaxial growth process, which in return deeply affects the resulting dislocation density and dislocation plasticity mechanisms. These latter, tailor the nanomechanical properties of GaN samples and the indentation-induced deformation behavior.

1. Introduction

III-V nitride semiconductors, such as GaN, AlGaN and InGaN have attracted considerable attention because of their wide band-gap and wavelength in the range of red to ultraviolet, for the fabrication of optoelectronic devices, optical detectors, semiconductor lasers, and other broad application spectrum [1,2].

In previous decades, intensive researches have been focused on GaN thin films in industry and academia laboratories owing to its high physical properties and its sustainability with low environmental impact [3–5]. Besides, the mechanical characteristics of GaN materials are also key factors for their successful application, since for instance, the contact loading during fabrication or packaging can seriously damage the devices' performance. Likewise, GaN based devices experience large thermo-mechanical strains, that affect their properties in service, besides to growth strains that are inherent during GaN crystal growth and heat treatment. The knowledge of GaN mechanical properties and understanding the elementary mechanisms responsible of nanoindentation-induced plastic deformation in semiconductors is of paramount importance for the fabrication, design and service of GaN-based devices [6].

In last decades, nanoindentation tests have been widely used as a powerful tool for probing the mechanical properties and behavior of materials within the atomic scale ranges [7,8]. Oliver and Pharr proposed an analysis method to compute the hardness and Young's modulus from the load–displacement curve obtained from nanoindentation tests using Berkovich indenter [7,9]. During nanoindentation, the load–displacement curve is marked by initial branch attributed to an elastic behavior with fully reversible deformation [10]. By continuously increasing the load, the onset of the plastic deformation (irreversible deformation) appears in general by the observed pop-in event or excursion in depth. The first pop-in events were observed on electro-polished surfaces of gold, copper and aluminum by Gane and Bowden [11]. This phenomenon was also commonly observed in several indented semiconductor materials [12–14]. Nevertheless, the threshold of plastic deformation is not usually revealed by the appearance of such

* Corresponding author.
E-mail address: zohra.benzarti@fss.usf.tn (Z. Benzarti).

https://doi.org/10.1016/j.apsusc.2021.152188
Received 22 April 2021; Received in revised form 5 November 2021; Accepted 9 December 2021
Available online 14 December 2021
0169-4332/

phenomenon and the elastic–plastic transition occurs unperceived without any discontinuities on the load–displacement curve [15]. The origin of this difference between the presence of pop-in events and their absence is not clearly understood at present.

Previous researches have reported on the determination of mechanical characteristics of GaN thin films. Tsai et al. [16] reported on Berkovich nanoindentation-induced deformation of GaN thin films grown using MOCVD process on a-plane sapphire substrate and demonstrated that pop-in event is related to the formation and propagation of dislocations, rather than by indentation-induced phase transformation. Later, Fujikane et al. [17] performed strain rate controlled nanoindentation test on bulk GaN crystals with large range of indentation load velocity. They investigated the effect of the load rates on the incipient plasticity of GaN crystals.

Even though, physical properties of semiconductors are affected by dislocations that are generated in lattice-mismatch during crystal growth process [18]; however, scarce works reported on thorough interpretation of various mechanical behaviors observed in semiconductors during nanoindentation-induced plastic deformation.

In this study, Berkovich nanoindentation tests, were performed on two GaN thin films grown on (0001) sapphire substrate by MOCVD under similar growth conditions, but with dissimilar carrier gases; H_2 for the first sample and N_2 for the second one. The carrier gas type for the GaN growth has attracted many interests [18,19], Amano et al. [20] initially adopted pure H_2 as the carrier gas. Later, Cho et al. [21] adjusted the carrier gas from H_2 to pure N_2 for GaN growth. The effect of carrier gas was studied on the structural, morphological, optical and electrical GaN epilayer characteristics [2,21,22].

Although of these interests in the carrier gas effects on physical properties of GaN films, to the best of our knowledge, the specific dislocation mechanisms that tailor the nanomechanical behavior and properties associated to the impact of carrier gas are not yet clearly addressed and well understood. In this framework, the present research provides a systematic investigation of the carrier gas H_2 and N_2 effect on nanomechanical properties and behavior of wurtzite GaN thin films grown by MOCVD. We attempt to shed some lights on the relations between the physical and mechanical features of GaN epilayers to understand their perceived dissimilar nanomechanical behaviors. This endeavor is a fundamental challenge, because it might contribute to deeply understand the nanoindentation-induced deformation mechanisms and then offers to fabricated GaN films the target physical and nanomechanical properties, leading to achieve high-performance optoelectronic devices based on nitrides.

2. Experimental details

GaN samples were prepared either with hydrogen (H_2) or with nitrogen (N_2) as carrier gas during growth process at 1100 °C. These GaN films were grown on (0001) *c*-plane sapphire substrates by metalorganic chemical vapor deposition (MOCVD) technique. Trimethylgallium (TMG) and ammonia (NH_3) were only used as precursors of gallium and nitrogen, respectively. During the growth process, and for each sample, a buffer layer of GaN (30 nm) have been deposited using a different carrier gas (either H_2 or N_2) under sapphire substrate. The thickness attained for both GaN samples is 2 μm. To seek for simplicity of the presentation, more details regarding the growth conditions are reported elsewhere [2,22].

In order to analyze the residual stresses within both GaN samples, micro-Raman spectroscopy (RS) and photoluminescence (PL) were performed. The used PL excitation source is the 325 nm (3.81 eV) wavelength line of an He-Cd laser of 10 mW power. Structural properties were investigated and dislocation density was revealed using HRXRD technique. Hall effect measurements (the standard Van der Pauw configuration) were used to obtain the electric properties and to attempt to correlate them with the presence of defects that influence the nanomechanical properties of GaN samples. The surface morphology of both GaN samples was assessed using atomic force microscopy (AFM) technique.

Nanoindentation tests were performed using nanoindentation instrument (NanoTest NT1, NanoMaterials, Ltd) equipped with a diamond pyramid-shaped Berkovich-type indenter. The three-sided pyramidal Berkovich shape has a half angle of 65.3°. The nanoindentation system was fully calibrated using fused silica as a standard sample prior to the measurements.

The tip-end curvature radius of Berkovich indenter was also determined using Hertzian analysis and found equal to 400 nm. Nanoindentation tests were performed at room temperature and atmospheric pressure, in the load rate-control mode up to the maximum loads P_{max} of 10 mN and 15 mN. At least sixteen independent tests were carried out on each sample to assess the reproducibility of the tests. At the maximum load, the indenter was maintained at a constant load for a dwell period of 30 s for the thermal drift reason. Each indentation was separated by 30 μm to avoid possible interferences between neighboring indents. It is worth to mention that all indentation depths are less than 10% of the film thickness, where the sapphire substrate effect on the characterized properties of GaN films is negligible. In addition, scanning electron microscopy (SEM) was used to observe and analysis the indentation imprints for both GaN samples. Using Vickers microhardness test, the length of generated cracks was measured to evaluate the fracture toughness K_{IC}.

In a final step, nanoindentation tests were carried out at four loading rates, 0.3 mN/s, 0.5 mN/s, 1 mN/s and 3 mN/s, to study the mechanical behavior of GaN samples undergoing an increase of loading rates.

3. Nanoindentation test analysis method

Hardness and Young's modulus are the most frequently mechanical properties extracted from nanoindentation testing. Oliver-Pharr's method is the most widely used one to extract these properties from load – displacement curves [9].

Hardness is defined as the ratio of the maximum load to the projected area of the indentation, denoted by A_c:

$$H = \frac{P_{max}}{A_c} \tag{1}$$

where, P_{max} is the maximum load and A_c is the projected area.

For a perfect Berkovich indenter, the projected area (contact area) is given by:

$$A_c = 24.5\ h_c^2 \tag{2}$$

where h_c is the contact depth and can be calculated as follows:

$$h_c = h_{max} - \varepsilon \frac{P_{max}}{S} \tag{3}$$

where, h_{max} is maximum depth, S is the contact stiffness and ε is a constant depending on the geometry of indenter. For Berkovich indenter tip $\varepsilon = 0.75$.

The reduced elastic modulus of the film is dependent on the contact stiffness S and on the projected area, then it is defined as follows:

$$E_r = \frac{1}{2\beta}\sqrt{\frac{\pi}{A_c}}S \tag{4}$$

where, $S = dP/dh$ is the slope of unloading curve at the maximum load point and β is the shape constant equal to 1.034 for Berkovich indenter.

The relationship between the elastic modulus of the tested film, the indenter and the reduced modulus is expressed by:

$$\frac{1}{E_r} = \frac{1-\nu^2}{E} + \frac{1-\nu_i^2}{E_i} \tag{5}$$

where (E, ν) and (E_i, ν_i) are the Young's modulus and Poisson's ratio

of the film and the indenter, respectively. For Berkovich diamond indenter, the Young's modulus and Poisson's ratio are given respectively by$E_i = 1141$ GPa and$\nu_i = 0.07$ [7].

Oliver and Pharr [7] found that the unloading curve is usually not linear, and it can be fitted using a power-law relation:

$$P(h) = \alpha\left(h - h_f\right)^m \tag{6}$$

where, P is the contact force, h is the indenter depth, h_f is the residual depth after indenter withdrawn, and α and m are power-law fitting constants.

Fig. 1 displays a typical load–displacement curve of nanoindentation test, where the contact stiffness S is shown. In certain conditions, it is interesting to assess not only the Young's modulus and hardness at a given depth, but also to evaluate the mechanical properties versus indenter depth. Indeed, the obtained results are rich of information and display the local plastic deformation behavior. Thus, in order to measure the nanomechanical properties as a function of the indenter penetration, a set of nanoindentation tests should be carried out at several indentation stepwise depths. As an alternative to this onerous method, the continuous stiffness measurement (CSM) emerges as technique to continuously measure the dynamic contact stiffness during the nanoindentation test. However, this technique is not always available and needs somehow fine adjustment [23]. Instead, in this work, we developed a new approach to compute the contact stiffness continuously as a function of the penetration depth using only a single load–displacement indentation curve performed for a given maximal load (P_{max}). Therefore, the mechanical properties are derived as a function of the depth.

In this new method, starting from a single measured load-unload displacement curve obtained at a maximal load $P_{\max}$. The measured load–displacement curve is subdivided into k-intervals of Δh length, as similar as a multiple load–displacement curves obtained at increased load P_i (see, Fig. 1). This method is based on the assumption of a purely elastic unloading path, which is properly justified for some kind of materials, where their mechanical behavior is time-independent. In this case, the unloading curve is fitted by the power-type law given in Eq. (6), as can be suggested by Oliver and Pharr [7]. In order to corroborate the elastic unloading path assumption, multi-cyclic nanoindentation was carried out at a maximal load of 15 mN on both GaN samples. One can see that for five achieved cycles, the loading path of the next cycle matches with the unloading path of the previous cycle, as shown in Fig. 2. These results provide a very strong evidence that this kind of materials obey a purely elastic unloading path.

The derived unloading curve corresponding to the load P_i is the branch of the measured unloading curve translated by a depth increment Δh to intercept the measured loading at the P_i load value. For each load value P_i, the contact stiffness S_i is the slope obtained at the maximal load P_i; where ($i = 1..k$) corresponds to the number of the increment loads. As the α,m and h_f parameters are initially determined by fitting the measured unloading curve, the contact stiffness S_i is calculated at the point (P_i, $h_i + \Delta h$) on the measured unloading curve using the following relation $S_i = \alpha m((h_i + \Delta h) - h_f)^{m-1}$. This contact stiffness S_i is assigned to the point (P_i, h_i) on the unloading curve (i.e., the branch of the measured unloading curve), where P_i and h_i are the maximal load and depth at the i^{th} point of the measured loading curve. This calculation procedure is applied to determine the different contact stiffness at different depth points along the loading curve. This is essential to calculate the contact depth h_c (see, Eq. (3)), then to obtain the contact area A_c, which enables to determine the harness H and the reduced Young's modulus E_r.

Commonly, indenters used in nanoindentation are imperfect by nature, that means the indenter tip feature is not perfectly sharp and has an imperfection assimilated to a round end defined by a tip radius. Hence, the Eq. (2) expresses the projected contact area along with contact depth

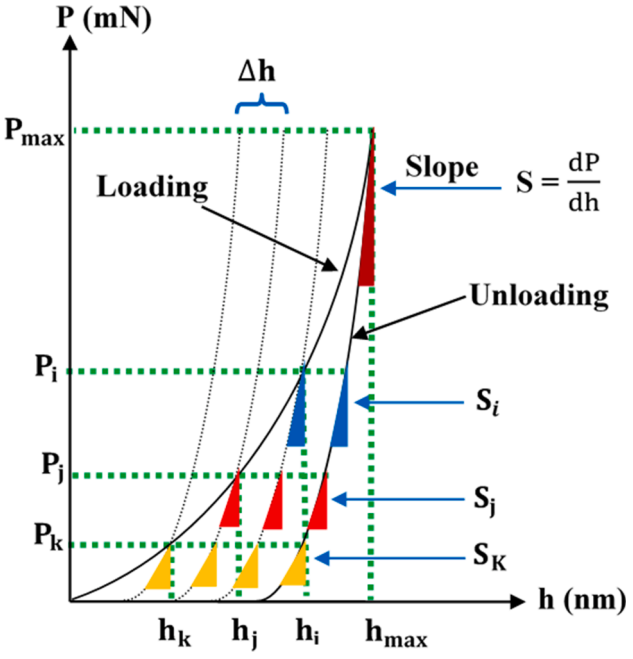

Fig. 1. Schematic illustration of typical load–depth curve obtained in nanoindentation and the definition of the contact stiffness at different loading increment based on the assumption of purely elastic unloading.

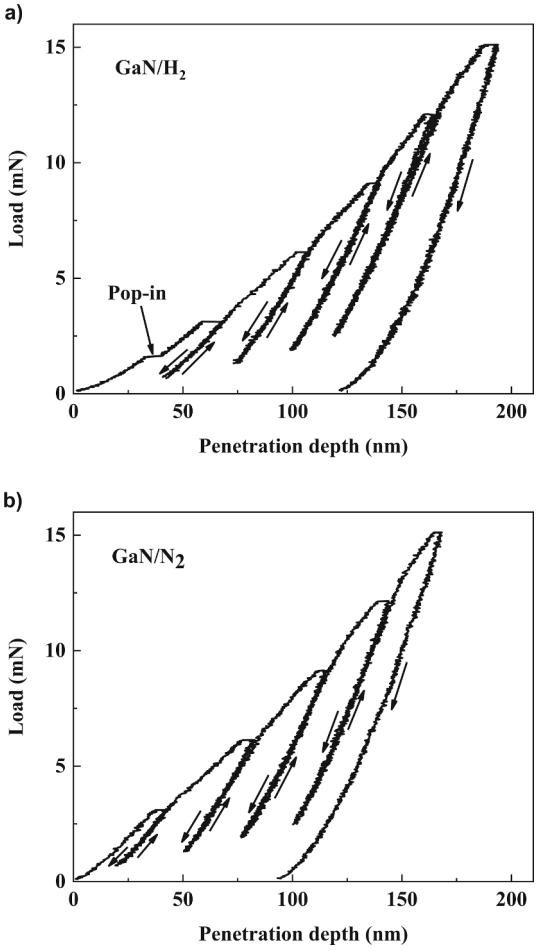

Fig. 2. Plots of experimental multi-cyclic nanoindentation load- displacement curves obtained with Berkovich indenter at a peak load of 15 mN: a) GaN/H_2; b) GaN/N_2. The loading path of the next cycle is overlying the unloading path of the previous cycle, illustrating a purely elastic unloading behavior.

for the Berkovich indenter is only a theoretical assumption, which underestimates the effective contact area. Actually, to take account of the indenter tip imperfection in the determination of the projected contact area, Oliver and Pharr have proposed an empirical formula, given as follows [7]:

$$A_c = f(h_c) = 24.5h_c^2 + C_1h_c + C_2h_c^{1/2} + \ldots + C_8h_c^{1/128} \quad (7)$$

where, C_1 through C_8 are the fitting constants obtained during the calibration process using fused silica with perfectly known mechanical properties.

4. Results and discussion

4.1. Physical properties of GaN samples

Commonly, the buffer layer deposited on sapphire substrate at low temperature (~600 °C) undergoes annealing stage, where the temperature increases to prepare the main GaN growth process at high temperature (~1100 °C). During buffer layer annealing, the surface morphology of the buffer layer is affected by carrier gas, among other factors [18]. For instance, using H_2 carrier gas, the GaN buffer layer was transformed into low density isolated nuclei, which were etched by H_2 at hot temperature (see, Fig. 3a). The etched GaN buffer layer was partially scattered to form large size GaN islands [24]. These islands have grown larger and spread out to coalesce with neighboring larger islands during the start-up of the hot temperature GaN growth. This growth regime is commonly designated by a three-dimensional growth mode (3D), which was observed for GaN grown with H_2 carrier gas [22,25]. In this case, relatively long duration was necessary for the islands to expanse laterally and to swap the 3D growth mode by a complete 2D lateral growth regime, which subsequently has led to a smoother surface, as shown in Fig. 3c.

In contrast, using N_2 carrier gas, the produced density of nuclei in GaN buffer layer was higher with reduced nuclei size during the annealing process, as shown in Fig. 3b. The GaN nuclei coalescence was closely immediate owing to this narrow neighborhood of small islands that were narrowly close. This 2D growth mode was achieved layer by layer along the total growth process of GaN/N_2 epilayer at hot temperature (see, Fig. 3d).

Commonly, the analysis of AFM data gives to quantitative information on the surface roughness. Root-mean square roughness R_{RMS} is defined as standard deviation of the surface height profile from the average height. R_{RMS} was calculated using the following equation:

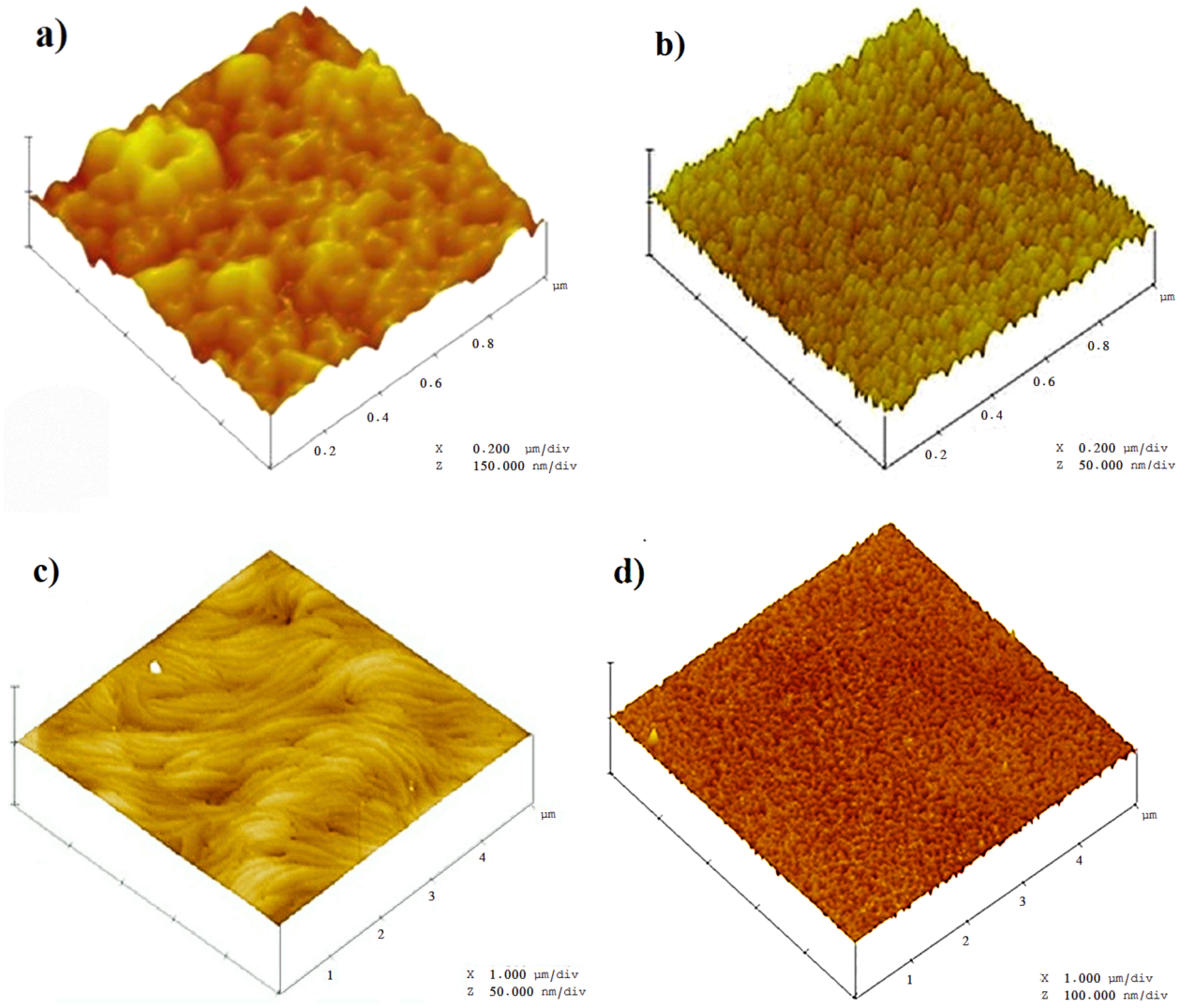

Fig. 3. AFM images of GaN buffer layer after annealing at 1100 °C with: a) H_2 carrier gas; b) N_2 carrier gas. AFM images of GaN epilayers: c) GaN/H_2 film; d) GaN/N_2 film.

$$R_{RMS} = \sqrt{\frac{1}{N}\sum_{i=1}^{N}(z_i - \bar{z})} \quad (8)$$

where, N is the number of data points, z_i and $\bar{z}$ are the height of i^{th} data point and the average height of the image, respectively.

For GaN/H_2 sample the R_{RMS} roughness value is equal to 0.5 nm and for GaN/N_2, R_{RMS} roughness was found equal to about 5 nm.

Indeed, the coalescence time is greatly reduced compared to the growth of GaN/H_2 sample [2]. This morphological difference between the buffer layers grown with H_2 and with N_2 was attributed to the difference in surface energy.

In order to assess the structural quality of both GaN films, it is necessary to compare the intensity and the full width at half maximum (FWHM) of their X-ray rocking curves. Fig. 4 **a** and **b** display the symmetrical (0 0 2) and asymmetrical (1 0 5) X-ray rocking curves of GaN/H_2 and GaN/N_2. These results indicate the high crystal quality of GaN/H_2 sample owing to its higher intensity and lower FWHM compared to GaN/N_2 sample. In fact, the measured rocking curve FWHM values of (0 0 2) and (1 0 5) are 259 arcsec and 262 arcsec for the sample grown in H_2 carrier gas atmosphere and 830 arcsec and 896 arcsec for N_2 atmosphere, respectively. This is often related to defects, mainly the density and distribution of threading dislocations (TDs) developed during the coalescence of the GaN growth process and mostly depending on the initial deposition conditions. The measured rocking curve FWHM for (*hkl*) reflection is given as follows [26]:

$$\beta^2(hkl) = \beta_\alpha^2(hkl) + \beta_\varepsilon^2(khl) \quad (9)$$

where, $\beta_\alpha(hkl)$ is the rocking curve broadening caused by angular rotation at dislocations and $\beta_\varepsilon(hkl)$ is the rocking curve broadening caused by the strains surrounding dislocations. Eqs. (10) and (11) relate the measured FWHM rocking curves to the dislocation density.

$$\beta_\alpha^2(hkl) = 2\pi ln 2 b^2 D = K_\alpha \quad (10)$$

$$\beta_\varepsilon^2(hkl) = K_\varepsilon tan^2\theta \quad (11)$$

where, b is the length of the Burger vector and D is the dislocation density. Fig. 4c displays a straight line which define a linear relationship between the $\beta^2(hkl)$ and the $tan^2\theta$ for five rocking curves at different value of angle θ, where the intercept is K_α and the slope is K_ε. The edge and screw dislocation densities were determined using Eqs. (10) and (11), respectively. The threading dislocation density is the sum of edge and screw type dislocation, for each one corresponds a Burger vector (b_{edge} = 0.3186 nm and b_{screw} = 0.5185 nm). In this context, it was found that the threading dislocation density is 5×10^9 cm^{-2} for GaN/N_2 and is equal to 2×10^8 cm^{-2} for GaN/H_2. These defect amounts are in accordance with the electron carrier mobility that are equal to 250 cm^2/V.s for GaN/H_2 sample and equal to 102 cm^2/V.s for GaN/N_2 sample, which are related to less defects in the GaN/H_2 epilayer compared to GaN/N_2.

GaN large isolated islands that were formed in the initial growth using H_2 carrier gas were found to be truncated shapes, on which the lateral growth was achieved during the coalescence of these large islands [18,25]. The threading dislocations likely blocked at the truncated facets and quench; consequently, reducing the propagation and the density of threading dislocations. It is worth to note that during the initial growth and along the annealing step, the formation of large islands was disseminated and etched by the H_2 carrier gas, as mentioned above; so, the distribution of threading dislocations throughout sample's surface and thickness may undergo an inhomogeneous redistribution.

In contrast at the initial growth step, the GaN/N_2 epilayer was featured by the formation of the small islands, in which the threading dislocations emerge at the layer surface, as a consequence of the strain relaxation effect and leading to high threading dislocation density in the sample. This statement was confirmed by the obtained dislocation density value [18].

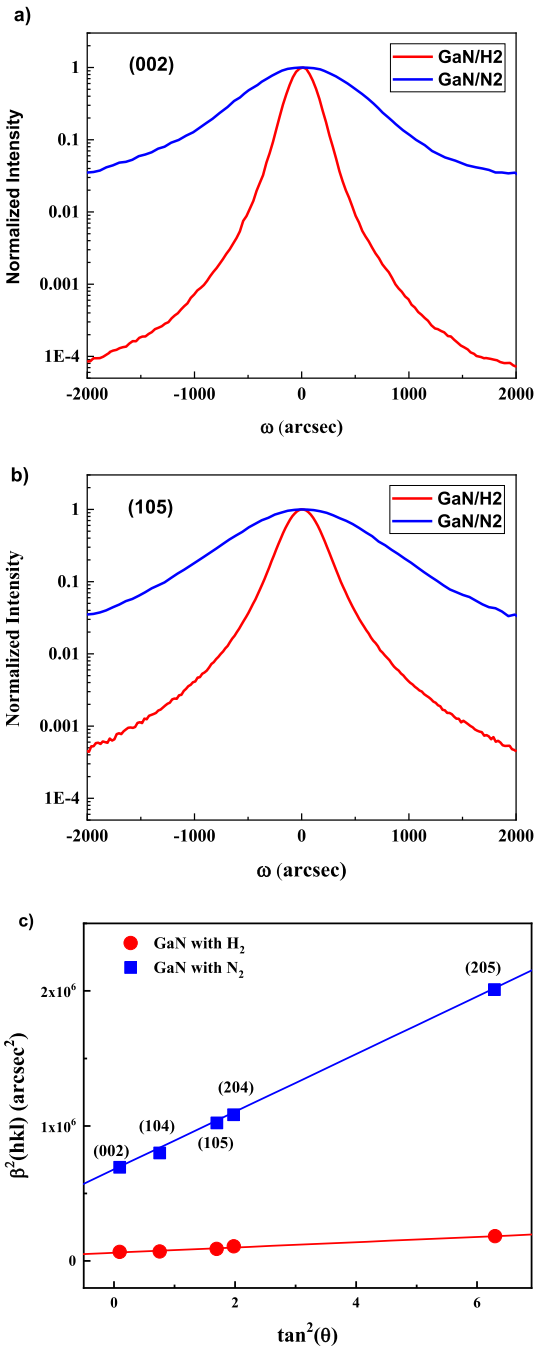

Fig. 4. a) Symmetric (0 0 2) rocking curve reflection; b) asymmetric (1 0 5) rocking curve reflection; c) square of rocking curve line width $\beta^2(hkl)$ versus $tan^2(\theta)$ for GaN/H_2 and GaN/N_2 samples.

Therefore, it is clear that the used carrier gas dictates the incipient density and distribution of dislocations and defects resulting from lattice mismatch of GaN, deposited on sapphire substrate [27,28] at the early stage of the growth (MOCVD) process.

An earlier report points out that the coalescence phase strongly influences the strain relaxation in the layer by inducing high threading dislocation density as well as the point defects [29].

In order to assess the stress states in GaN films grown using different carrier gas, actually micro-Raman spectroscopy is the suitable technique enabling this valuation. RS allowed to determine the crystalline quality and strain relaxation in the layer, which is directly related to the threading dislocation density appraised from FWHM rocking curves. The

intense E_2 phonon frequency mode [30,31] was used as reference peak to determine and compare the compressive biaxial stresses in both GaN samples. Fig. 5a shows Raman shift of the E_2 phonon mode for both GaN/H_2 and GaN/N_2 epilayers. It is easy to observe that $E_2^{(H_2)}$ phonon mode frequency for GaN elaborated with H_2 carrier gas is located at 570.04 cm^{-1} and the $E_2^{(N_2)}$ phonon mode frequency for GaN grown with N_2 atmosphere is positioned at 568.13 cm^{-1}. The dashed line refers to the strain-free frequency of the E_2 phonon mode for GaN bulk layer, which is situated at 566.34 cm^{-1} [21].

Based on these results, it is important to highlight that the two layers are subjected to compressive residual stresses, because they are on the right side of the bulk GaN position.

Moreover, these results show that the GaN/N_2 film is less compressed than that of the GaN/H_2 film. Indeed, the strain relaxation of the GaN/N_2 film is related to the increase of the threading dislocations embedded in the sample, as mentioned in previous reports [32]. In other words, the GaN/H_2 film experienced less strain relaxation resulting in less threading dislocation density, as confirmed by the measured density dislocation for both GaN samples. The thermal expansion coefficients and lattice mismatch at the film and substrate interface are generally the principal origins in the difference of the strain relaxation between the two GaN samples. Moreover, it appears that the strain relaxation of the epilayers is inhomogeneous across the thickness of samples. Indeed, the compressive residual stresses are smaller close to the substrate than to near the GaN film surface, as reported by Cho et al. [21].

Besides, the structural properties of GaN thin films related to the residual stress was investigated using PL at temperature of 5 K by identifying the excitonic line position. Fig. 5b shows for GaN/H_2 higher PL peak intensity, with the excitonic line position of 3.483 eV, compared to that obtained for GaN/N_2 (3.479 eV). The dashed line refers to the strain-free excitonic line position for GaN bulk layer, which is placed at 3.469 eV [33]. The difference in the peak PL position is related again to the dissimilar compressive residual stress states for both GaN samples. As known, for GaN grown on sapphire, the excitonic lines shift toward higher energies as the residual stress in the layer increase [34]. Moreover, the FWHM of the excitonic peak for GaN/H_2 epilayer (FWHM (H_2) = 4 meV) is smaller than for the other sample (FWHM (N_2) = 10 meV). Once again, these results confirm the superiority of the crystalline quality of GaN/H_2 epilayer compared to GaN/N_2 sample. Consequently, as above stated, it is clearly shown that both Raman and PL results are in well accordance; hence, the crystalline quality and the stress relaxation of both GaN samples were efficiently established. Moreover, these results are in good correlation with the measured threading dislocation density obtained by rocking curve reflections. These findings are in good agreement with literature reports [35].

Currently, the key question is what are the consequences of the used carrier gas on the nanomechanical behavior and properties of GaN epilayers? In the following, we show the nanomechanical results and based on the analysis of the indentation induced-deformation curves, we attempt to interpret the nanomechanical features and behavior in relation with the physical properties of both GaN samples.

4.2. Nanomechanical properties of GaN samples

Fig. 6a and b show the loading-displacement (*P–h*) curves for GaN films, grown using N_2 (GaN/N_2) and H_2 (GaN/H_2) as carrier gases, respectively. Indentation experiments were carried out at two maximal

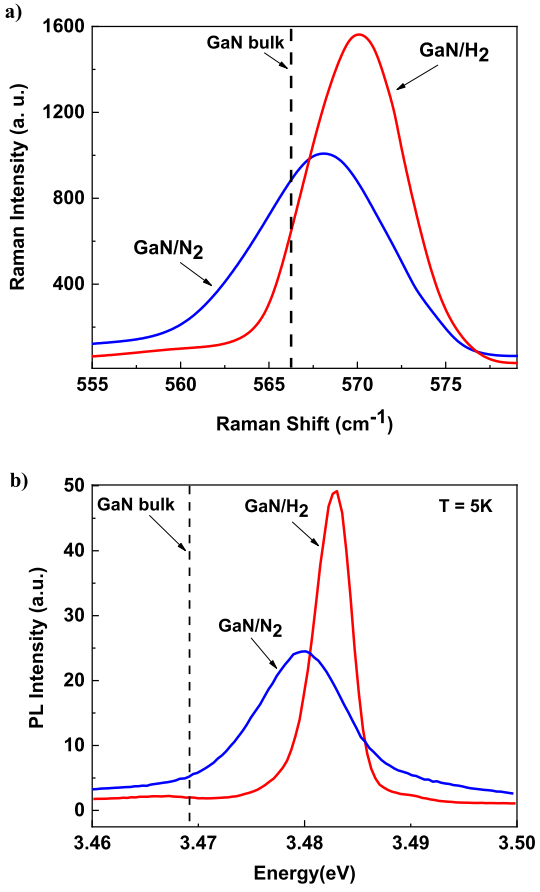

Fig. 5. a) Raman spectra at room temperature; b) PL spectra measured at 5 K obtained for both GaN/H_2 and GaN/N_2 epilayers.

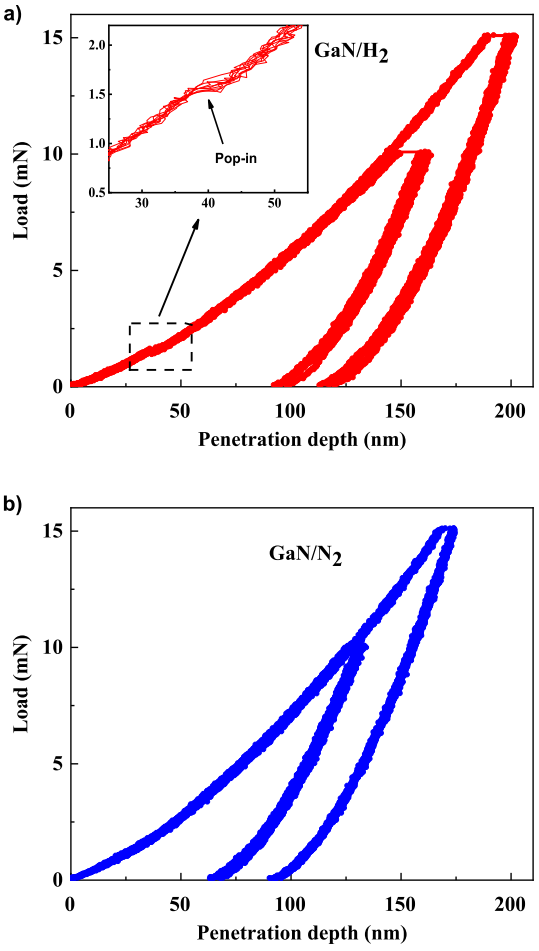

Fig. 6. Load–displacement curves of 16 nanoindentation tests obtained at maximal load of 10 mN and 15 mN for: a) GaN/H_2 film (red curves); b) GaN/N_2 film (blue curves).

loads, 10 mN and 15 mN. The indenter was withdrawn using the same loading rate of 0.3 mN/s as in the loading step. It is worth to note, that for both samples, the 16 nanoindentation curves are overlapped demonstrating the reproducibility of the experiments.

By analyzing Fig. 6a and b, one can observe that the loading curves for GaN samples are different. Fig. 6a displays the occurrence of the pop-in event for GaN film grown using H_2 carrier gas. This first pop-in event, corresponds to a sudden burst during the loading curve, which occurs at low load, designed by critical load of$P_{cr} = 1.48$ mN (pop-in plateau) for a penetration depth of about 40 nm. The pop-in length of the horizontal plateau is about 7.2 nm. The dissipated energy for the creation of this pop-in event was evaluated at 8.3×10^{-12}J. It may be noted that previous results reported by Jian et al. [36] are in agreement with the current findings. Moreover, at peak loads (i.e., 10 mN or 15 mN) and during the dwell period (30 s), the indenter continued to penetrate into both samples. The aim of holding the peak load for a sufficient period of time was to avoid any effect of the thermal drift on the computed hardness and Young's modulus and to totally guarantee the material's elastic recovery. Additionally, one can observe that due to its local resistance to plastic deformation, the penetration depth for GaN/N_2 film was lower than that observed for the GaN/H_2.

Based on preliminary analysis of these results, it is more likely to mention that the usage of H_2 gas for the elaboration of GaN films contributes to a certain ductility and easiness to penetrate into the sample. In contrast, the usage of N_2 carrier gas to grow GaN films, enhances the indenter penetration resistance into the sample. These observations were corroborated by the calculated plastic work W_p for both GaN samples at a maximal load of 10 mN. The calculated plastic works are $(368 \pm 10)\times10^{-12}$J and $(265 \pm 10) \times10^{-12}$J for GaN/$H_2$ and GaN/N_2, respectively. This difference in the plastic work reveals the enhanced ductility of GaN/H_2 film compared to GaN/N_2. Thus, it is of paramount importance to understand the foundations behind such distinct behavior of GaN samples. Next, based on thorough analysis of qualitative and quantitative results, further interpretations of the observed distinguish nanomechanical behavior of the elaborated GaN samples would be possible.

The usage of the developed method permitted to compute the Young's modulus E and the hardness H as function of penetration depth. Our chief aim by measuring the depth-dependent hardness of the GaN samples was to examine the presence or not of this dependence associated to the indentation size effect (ISE).

Fig. 7a and b show for both GaN samples, the evolution of these nanomechanical properties obtained from the average curve representing the 16 experimental indentation tests carried out at maximal load of 10 mN. As can be seen, depth-dependent Young's modulus and hardness are larger for GaN/N_2 than that for the GaN/H_2. Fig. 7a shows Young's modulus for GaN/N_2, which was observed continuously decreasing along with the penetration depth. In contrast, for the GaN/H_2 sample, the evolution is practically constant around an average value of 310 GPa and almost independent of the magnitude of the local plastic deformation in the range of penetration depth of 50 nm to 150 nm. The peak depicted in these curves was associated to the pop-in event observed for this sample. Fig. 7b shows the evolution of the hardness as a function of the penetration depth for both GaN samples. One can observe the constancy of the hardness along with the penetration depth after the initiation of the pop-in event (i.e. beyond almost 40 nm of depth), for the GaN/H_2. However, for the GaN/N_2, it can be seen the gradual increase of the hardness as a function of the penetration depth. This latter increases started after a depth of about 30 nm, which indicates the onset of the plastic deformation.

The incipient plasticity is attributed to a maximal shear stress at which plastic deformation starts locally beneath the indenter tip. Using the Johnson's model [37], the maximal shear stress was calculated and given by the following equation:

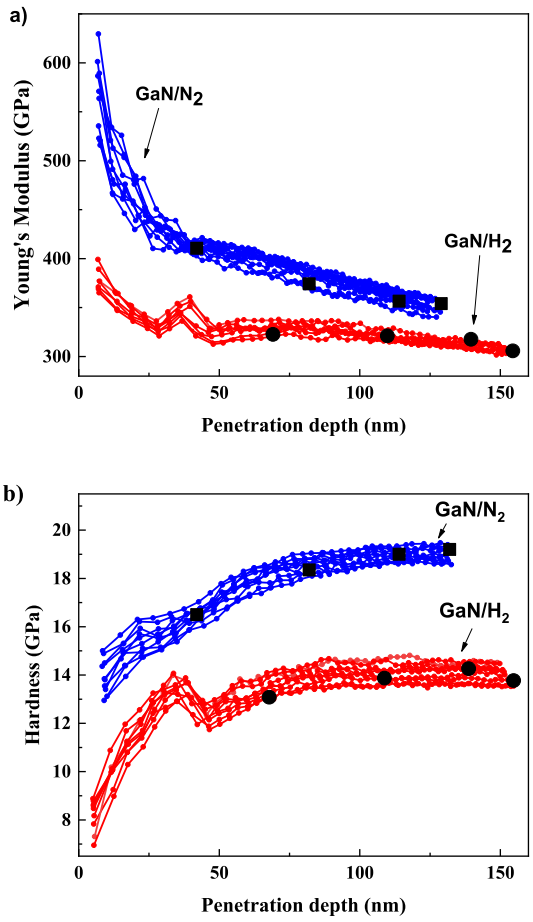

Fig. 7. a) Young's modulus; b) hardness as a function of penetration depth of GaN/H_2 and GaN/N_2. Black square and disk solid symbols refer to Young's modulus and hardness, measured based on single load–displacement curves obtained at various maximum loads.

$$\tau_{max} = 0.31\left(\frac{6P_{cr}E^2}{\pi^3 R^2}\right)^{1/3} \quad (12)$$

where P_{cr} , E and R are the critical indentation load, the Young's modulus and the radius of the indenter tip, respectively. This critical load corresponds to the maximal load at which the local plastic deformation is initiated underneath the indenter tip. The calculated maximal shear stresses induced-plasticity are 17.3 ± 0.6 GPa and 16.2 ± 0.6 GPa for GaN/H_2 and GaN/N_2, respectively.

At the maximal load of 10 mN, the average values of Young's modulus E, the Coulomb's or shear modulus G and the hardness H are 313 ± 6 GPa, 125 ± 2 GPa and 13.7 ± 0.6 GPa for GaN/H_2 and 356 ± 4 GPa, 142 ± 3 GPa and 19.5 ± 0.4 GPa for GaN/N_2, respectively.

As Taylor hardening model represents a straightforward relationship between the dislocation density and the indentation hardness, since the hardness is proportional to the square root of the dislocation density [38]. Consequently, the measured hardness was found in accordance with Taylor model prediction because the dislocation density found for the GaN/N_2 epilayer is higher than for the GaN/H_2 film.

In addition, Fig. 7 shows the plotted values of Young's modulus and hardness (Black square and disk solid symbols) obtained from the multi-cycle indentation tests. One can see the good agreement between the provided results using the new method, developed to calculated the stiffness and then to determine the nanomechanical properties as a function of the indenter depth, and those obtained from single load–displacement curves. This represents a quantitative validation of the proposed method to calculate continuously the evolution of

nanomechanical properties along with penetration depth using a single nanoindentation test.

Table 1 presents nanomechanical properties of GaN thin films reported in previous studies of literature and the results obtained in this study. It clearly depicts discrepancies between the reported nanomechanical properties for GaN films. This scatter of these nanomechanical properties obtained by various nanoindentation tests is mainly attributed to the specific tip – surface contact configuration and to the different stress distribution inherent into specimens. This is somewhat owed to elaboration conditions, to defect interactions with indenter tip inducing local plastic deformation and to the used indenter tip-type [39].

4.3. Dislocation mechanism scenarios correlated to the epitaxial growth processes

Attaining this stage in the investigation, we attempt to thoroughly analysis the correlation between the experimental nanomechanical properties and the type of carrier gas used in the GaN growth process. As abovementioned, GaN/H_2 sample showed a first pop-in event, while for the GaN/N_2 sample, no pop-in events were observed along the loading curve. In fact, several possible interpretations for the manifestation of pop-ins were reported in literature. The occurrence of pop-ins was sometimes related to phase transformation [44], initiation and propagation of micro-crack [45] and initiation of plastic deformation, marked by the transition between elastic to plastic of the strained locally volume underneath the indenter [46,47]. In the present paper, the latter explanation is very prospected, as it attributes pop-in events to a mechanism of homogeneous dislocation nucleation of loops. Microscopical investigations have revealed the homogeneous nucleation of dislocations process during nanoindentation [48–50]. This dislocation mechanism was also strongly supported using molecular dynamic simulations (MDS) defect free-volume subjected to critical shear stress, which activates slip systems and then induces the nucleation and emission of dislocation loops [51]. In other words, homogenous dislocation nucleation mechanism was the only possible scenario if no mobile dislocations already existed in the sample close to the indenter. This is likely encountered in some materials featured with lower pre-existing mobile dislocation density that were not emerging at the sample surface. Previous works reported that many factors influence on the mechanical behavior and particularly on the initiation of plasticity in thin films [44,52,53]. Indeed, the crystallographic texture, the presence of surface roughness [54,55], interstitial atoms, density and distribution of pre-existing dislocations [6] and the influence of indenter tip geometry [39] are among the aspects that influence the appearance or disappearance of the pop-ins in material indentation. According to literature, dissolved interstitial atoms in crystalline materials, featured by shallow dislocation density, influence the pop-in event occurrence [50]. Moreover, the pop-in event positions were also strongly influenced by the interaction between the pre-existing threading dislocation density and the interstitials, where these latter pinned and locked of pre-existing mobile dislocations [49,56]. Unlocking of pre-existing dislocations that were pinned by interstitials can produce also the appearance of pop-ins [57].

Table 1
Nanomechanical properties of GaN thin films compiled from literature with findings of the present work.

References		E(GPa)	H (GPa)	τ_{max}(GPa)
Jian [36]		314.93 ± 40.58	19.34 ± 2.13	–
Tsai [16]		286 ± 25	19 ± 1	6.3
Chien [40]		286.12 ± 25.34	19.31 ± 1.05	–
Kucheyev [41]		233	13.4	11.5
Fujikane [42]		323.8	20.0	18.9 ± 1.3
Huang [43]		333.6 ± 2.7	19.04 ± 0.23	–
This work	GaN/N_2	356 ± 4	19.5 ± 0.4	16.2 ± 0.6
	GaN/H_2	313 ± 6	13.7 ± 0.6	17.3 ± 0.6

In this context, for a better argument foundation of the observed pop-ins phenomenon in GaN/H_2 sample, we attempt to evaluate the density of dislocation loops using the classical dislocation theory. Actually, the free energy U required for homogeneous emission of circular dislocation loop of radius r and Burgers vector magnitude b, by applying the shear stress τ_{max} to initiate plastic deformation, is given by the following equation:

$$U = 2\pi r\gamma_{dis} - \tau_{max} b\pi r^2 \tag{13}$$

where γ_{dis} is the line energy of the generated dislocation loop. Indeed, the Eq. (13) is composed of two terms. The first term expresses the necessary energy to create one dislocation loop in free-defect lattice and corresponds to the increased lattice energy due to the nucleation of the circular loop. The second term represents the necessary energy as the external work for the expansion of the dislocation loop. The line energy γ_{dis} is given by the following equation:

$$\gamma_{dis} = \left(\frac{2-\nu}{1-\nu}\right)\frac{Gb^2}{8\pi}\left(ln\frac{4r}{r_o} - 2\right) \tag{14}$$

where, G, ν and r_0 are the shear modulus, Poisson's ratio and the radius of the dislocation core of GaN/H_2 film, respectively. On one hand, the free energy U has a maximal value, when the dislocation loop radius attain a critical value r_c and on the other hand, it is in the similar order of the thermal energy $kT \sim 10^{-23}$J (k is the Boltzmann constant and T is the absolute room temperature) which is very small, $U(r_c) \sim 0$. Thus, by considering these conditions, the following relations are derived:

$$r_c = \frac{2\gamma_{dis}}{b\tau_{\max}} \text{and} r_c = \frac{\exp(3)}{4} r_o \tag{15}$$

Using these equations, the estimated critical and core radii for the dislocation loop are$r_c \sim 1.8$ nm and $r_o \sim 0.36$ nm for the GaN/H_2 film, respectively. The number of dislocation loops generated at the first pop-in is estimated using the ratio between the free energy which is estimated around of $U \sim 7 \times 10^{-17}$ J and the dissipated energy for the creation of this pop-in event (evaluated at 8.3×10^{-12}J). The obtained number of dislocation loops associated to the pop-in event is $\sim 10^5$ dislocation loops. This number is considered small and it is in accordance with the homogeneous dislocation nucleation mechanism [58], rather than with the collection activation of pre-existing mobile dislocation scenario (Dislocation cross-slip in GaN single crystal). Using this method and assuming that the total dissipation energy in the nanoindentation was completely transferred into the formation of dislocation loops with critical radius, the number of the formed dislocation loops is in the order of 5×10^6 dislocation loops. This value is regarded as an overestimation of what can be the upper limit of the number of the formed dislocation loops, when the total dissipation energy representing the area between the loading and unloading curves was used.

The GaN/N_2 indentation loading –displacement curve shows a different nanomechanical behavior of local volume deformed by shear stress underneath the indenter tip, compared to that observed for GaN/H_2 film. As reported in literature, the pre-existing dislocation density usually has a strong effect on the revelation or not of pop-in events [13,49,59]. Lorenz et al. [58] stated with a high degree of certainty that, the pop-in event will not appear for dislocation density higher than 10^9 cm^{-2} for high indenter tip radius. Herein, it is clearly noticed the absence of distinct pop-in event (see, Fig. 6b). This is commonly attributed to the interaction between the indenter tip and the high pre-existing mobile dislocation density. The high dislocation density encountered in GaN/N_2 film is $\sim 5 \times 10^9$ cm^{-2} and it is directly related to the epitaxial growth process using N_2 as carrier gas.

Consequently, the low or high pre-existing dislocation density (determined using X ray rocking curves), was generated and propagated since the early growth process of GaN samples. The growth mode (either 2D or 3D revealed using AFM images) is dictated by the used carrier gas-

type and therefore affects the residual dislocation density within samples. This variation of the pre-existing dislocation density contributes to the increase or decrease of the compressive stress, assessed using RS and PL techniques, as a consequence of the grade of strain relaxation achieved along with the crystal growth. During the nanoindentation test, the interaction between the indenter tip and the residual dislocations underneath the indenter was manifested by the generation and propagation of new dislocations according to the related dislocation mechanism. This latter is expressed on the load nanoindentation curve by the presence or not of pop-in events. Indeed, for high residual dislocation density, the collective movement and multiplication of mobile dislocations is the eminent dislocation mechanism-based plastic deformation. In contrast, for low residual density dislocation, the induced-plastic deformation, underneath the indenter tip, is mostly attributed to the homogeneous dislocation nucleation mechanism.

In order to illustrate the concept of the dissimilar dislocation mechanisms encountered in each GaN film during indentation test, Fig. 8 shows schematic representations (models) of dislocation mechanisms that can occur during the nanoindentation of GaN/H_2 (Fig. 8a) and GaN/N_2 (Fig. 8b**).** The dislocation mechanism is related to the incipient dislocation density and to the compressive strain state that were originated from the used carrier gas. In this study, we present this interpretation as a speculation of the most probable scenarios that might occur and enable us to understand the distinct nanomechanical behavior observed on GaN nanoindentation curves. The speculation of such dislocation mechanisms could be visually assessed using transmission electron microscopy (TEM) technique as a possibly future work.

4.4. *Fracture toughness assessment*

Nanoindentation test has proven to be a powerful technique to evaluate material's brittleness or resistance to fracture. The fracture toughness was evaluated using nanoindentation tests and is defined by Lawn–Evans–Marshall (LEM) model as follows [60].

$$K_{IC} = \alpha\left(\frac{E}{H}\right)^{1/2}\frac{P}{c^{3/2}} \tag{16}$$

where E is the Young's modulus, H is the hardness, P is the indentation load, c is the crack length and α is an empirical constant that depends on the geometry of the indenter (α = 0.016 for the Vickers 4-sided pyramidal indenter). This equation defines the relationship between the fracture toughness K_{IC} and the ratio of hardness to Young's modulus of a material (H/E) [61]. The higher ratio (H/E), the less fracture toughness K_{IC} is. Besides, the H^3/E^2 ratio is defined as suitable index to assess the ability of material to resist the plastic deformation of the material [62].

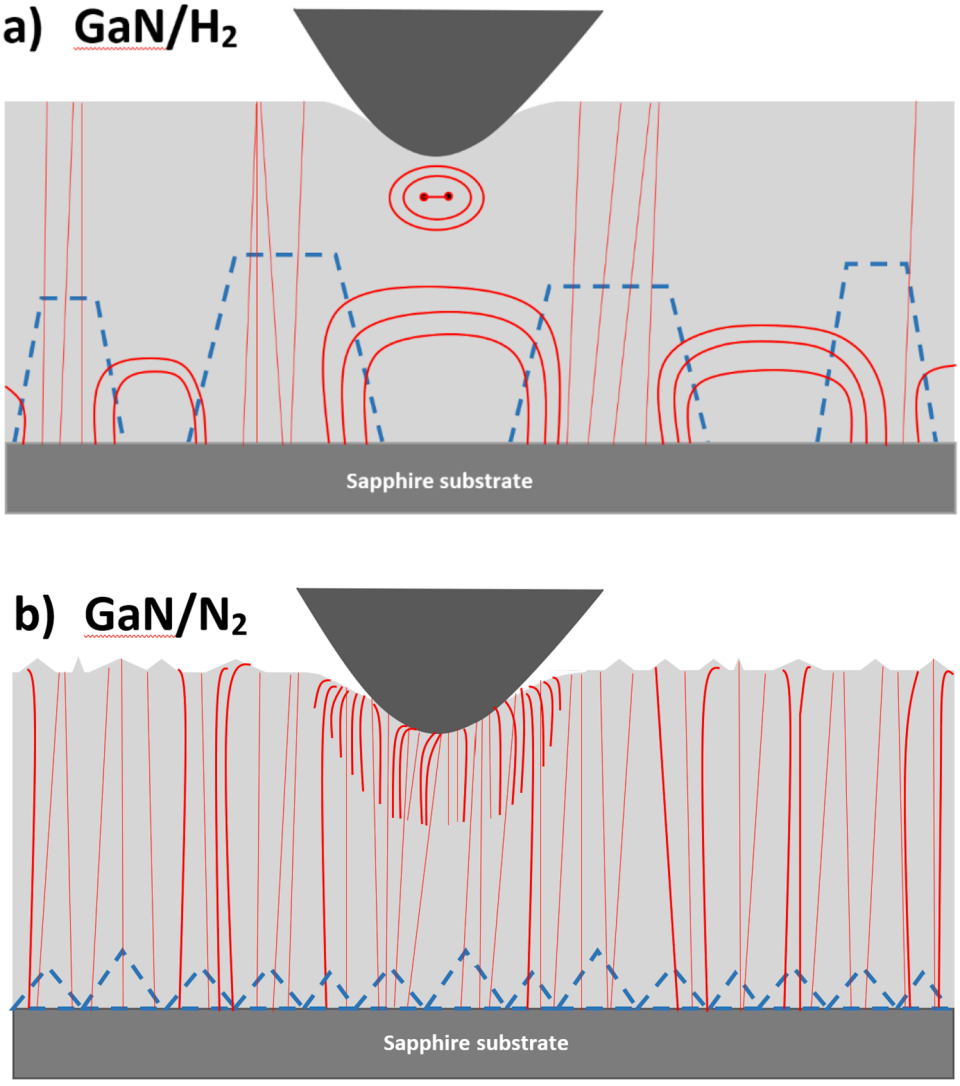

Fig. 8. Schematic representation of dislocation mechanisms responsible for the nanomechanical behavior observed in load–displacement curves of: a) GaN/H_2; b) GaN/N_2.

Fig. 9 shows the average variation of H/E and H^3/E^2 ratios as a function of the penetration depth for GaN/H_2 and GaN/N_2 films obtained at the maximum loading value of 10 mN.

This figure shows that starting from nearly 40 nm of penetration depth, H/E and H^3/E^2 ratios obtained for GaN/N_2 are higher than those obtained for GaN/H_2. This means that the fracture toughness K_{IC}, which is inversely proportional to the square root of (H/E) ratio of GaN/N_2 is lower than that of GaN/H_2. In other words, the probability of GaN/N_2 film fracture, when critical load of fracture was attained, is higher than for GaN/H_2 sample. Moreover, the increased penetration depth to produce larger plastic strains in GaN/N_2 required higher load increment compared to GaN/H_2. In fact, Fig. 9 clearly shows that for GaN/H_2, both (H/E) and (H^3/E^2) ratios are fairly steady around an average value; however, for GaN/N_2, they are increasing with penetration depth. In order to interpret these curve trends, we refer to the evolution of Young's modulus and hardness for both samples, as displayed in Fig. 7. For both GaN samples, hardness is around a steady value starting from around 50 nm of penetration depth (see, Fig. 7b).

However, for GaN/N_2 the decrease of its Young's modulus versus the penetration depth is higher (larger decreasing of the slope) compared to that for GaN/H_2 (see, Fig. 7a). Based on these findings, GaN/H_2 film shows a ductile behavior, where it is possible to undergo more plastic strains by applying locally sever shear stresses. In contrast, for GaN/N_2 sample, (where the majority of these dislocations emerged at the sample surface), the indenter tip interacts with the collective movement and multiplication of the activated pre-existing mobile dislocations resulting in higher dislocation density underneath the indenter tip. This may lead to an increase of the probability of the initiation of internal fracture, which can emerge to the sample surface as cracks. Indeed, the decrease of the Young's modulus along with the penetration depth for GaN/N_2 is synonym to a decrease of the material stiffness, which is attributed more likely to the formation of nano cracks that grow and coalesce to lastly lead to fracture. In order to quantitatively assess this behavior, the calculated fracture toughness was found equal to $K_{IC} = 0.85$ MPa $m^{1/2}$ for GaN/N_2, using LEM model given by Eq. (16). This sample showed failure and crack propagations for an applied load of 1962 mN using Vickers microhardness indenter (see, Fig. 10**a**). Moreover, the higher residual stresses and their inhomogeneous distribution within the thin film can significantly disturb the fracture behavior and scattered cracks appears around the imprint [63]. Nonetheless, this finding is comparable to the value obtained in literature and it is in the range between 0.7 and 1.0 MPa $m^{1/2}$ [64,65]. While in alike conditions, the GaN/H_2 loaded using Vickers microhardness indenter, no apparent of cracks was shown (see, Fig. 10**b**). However, it looks that a small pile up phenomenon is observed around the borders of the imprint, which reflects the large capacity of plastic deformation that can undergo the GaN/H_2 sample and reveals its higher ductile behavior. It is supposed that more loading force should be applied to likely attain failure and therefore cracks appearance.

To sum up the main results in this subsection, it is interesting to emphasis that crack phenomenon is attributed to the interaction and propagation of dislocation activities in the area of the indented surface. Whereas, the crack propagation is caused by highly strained field volume underneath the indenter and crystallographic properties of the material [45,66]. Therefore, the carrier gas used for GaN growth process plays a crucial role on the resistance of material to fracture underneath an indenter tip or simply to its fracture toughness value.

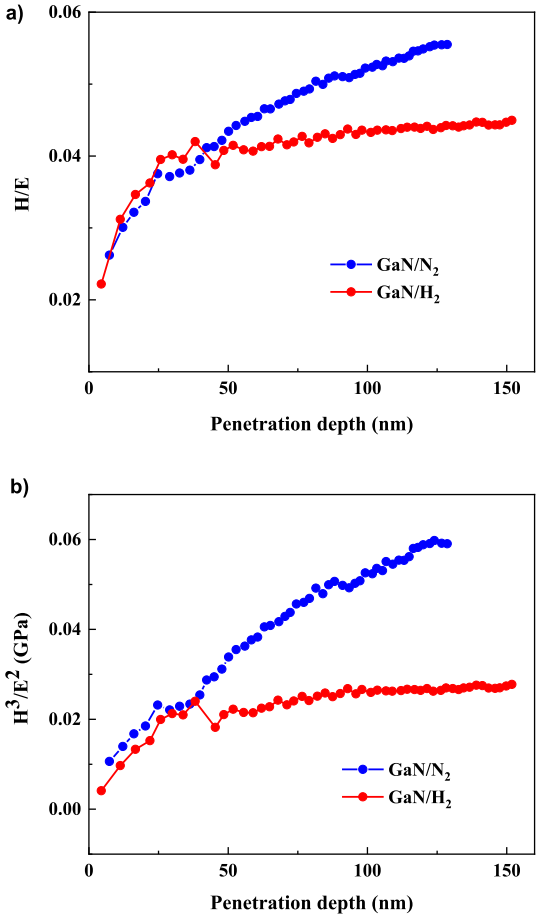

Fig. 9. a) H/E; b) H^3/E^2 variation versus penetration depth calculated for a maximum load of 10 mN, for both GaN films.

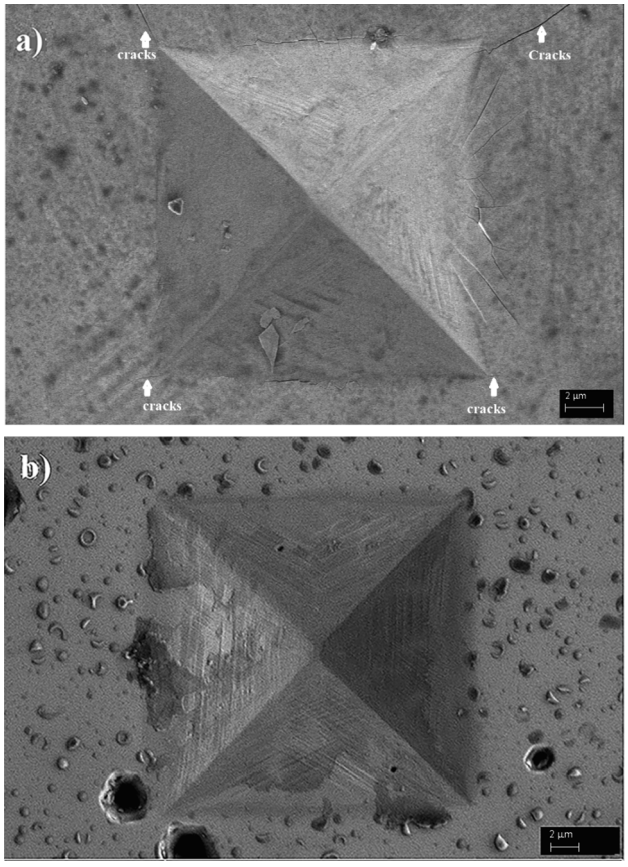

Fig. 10. SEM images of indented regions with a Vickers microhardness indenter at load of 1962 mN on the top surfaces of both GaN films: a) GaN/N_2 sample displays the cracks along corner and edges of the imprint; b) GaN/H_2 sample shows the pile-up phenomenon around the imprint boundaries.

4.5. Loading rate effect

Fig. 11 shows the load–displacement curves obtained at various loading rates, namely, 0.3, 0.5, 1, and 3 mN/s for both GaN thin films. One can distinguish that load–displacement curves for GaN/H_2 are sensitive to the loading rate. Moreover, the width of the pop-in plateau and the critical load are increasing with loading rate (see, Fig. 11a). For instance, 6 nm, 13 nm, 21 nm and 29 nm are pop-in plateau width, and the associated critical load are 1.48 mN, 4.27 mN, 6.13 mN and 8.46 mN, obtained for the following loading rates: 0.3 mN/s, 0.5 mN/s, 1 mN/s and 3 mN/s, respectively. As consequence, for GaN/H_2 the shear stress is loading rate-dependent. In addition, the work of pop-ins is increasing; so, the thermal activation of the homogeneous dislocation nucleation mechanism [67,68], which is responsible for the formation of loops that contribute to the increase of the density of dislocations, is getting higher along with loading rate. Therefore, the local volume of material underneath the indenter tip is featured by an increase of the hardness along with the loading rate rise. GaN/H_2 shows a strain hardening effect, which could be explained by the rise of loading branch slopes for the load–displacement curves with the increase of the loading rate. Such effect was not revealed in the investigated bulk GaN samples by Fujikane et al. [17].

In contrast, for GaN/N_2, the measured load–displacement curves at different loading rates are fairly overlapped, even for high loading rates, as higher as 3mN/s, (see, Fig. 11b). This assumes that the load associated to the onset of plastic deformation is almost the same and then loading rate-independent, therefore the maximal shear stress for the transition from elastic to plastic deformation is identical. In this case, it should be noted that the increase in the loading rate did not induce any increase of the sample hardness, i.e., the plastic deformation at high loading rate was induced by rapid movement of collective mobile dislocations that probably contributed to an increase of the material damage, due to its low fracture toughness K_{IC}, as previously mentioned.

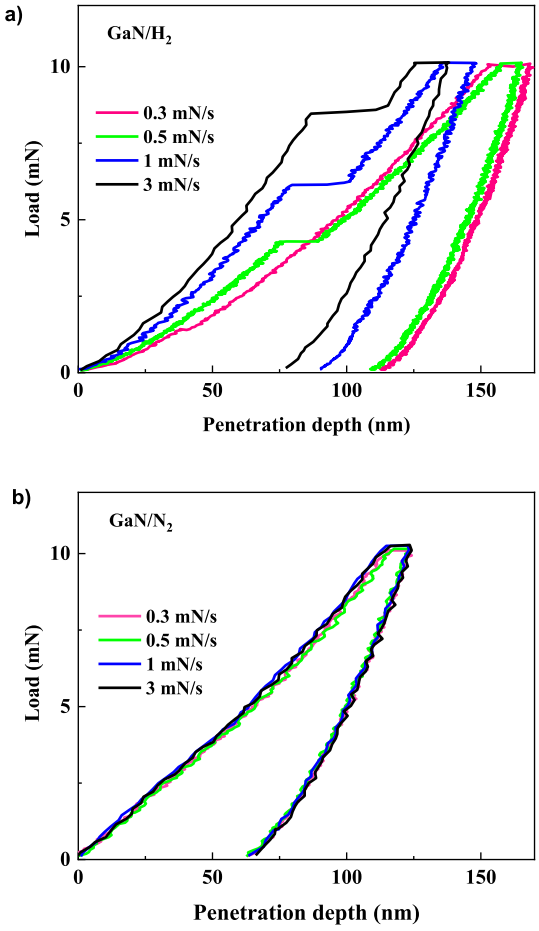

Fig. 11. Representative load–displacement curves of: a) GaN/H_2 epilayer, where the dynamic effect has an influence on the plastic onset and behavior; b) GaN/N_2, where no effect of loading rate was observed on the nanoindentation load-unload curves.

Table 2 lists for both GaN samples, the calculated maximum shear stress and the average of the plastic work associated to the range of the considered loading rates. One can observe the gradual rise of the maximum shear stress versus the increase of loading rate, for GaN/H_2 sample. However, the average plastic work is decreasing, which is synonym of losing its ductility. This means that the reduction of ductility along with the loading rate is attributed to an increase of the sample hardness, interpreted as work-hardening effect. In contrast, the maximum shear stress and the plastic work are loading-rate independent for GaN/N_2.

In order to quantitatively assess the Young's modulus and hardness evolution as function of the loading rate, these results are plotted in Fig. 12 for both GaN samples. For GaN/H_2, Young's modulus and hardness are increasing along with the loading rate. These results reveal its plastic hardening behavior. In the microscopic point of view, this is explained by the homogeneous dislocation nucleation mechanisms that create and emit dislocation loops in a sample with a low pre-existing dislocation density, as depicted in Fig. 8a. However, for GaN/N_2, it appears that the Young's modulus was decreased by increasing the loading-rate; that means, the local volume underneath the indenter tip was losing its stiffness, as shown in Fig. 12a. While, Fig. 12b shows that GaN/N_2 hardness was not undergoing a hardening behavior by increasing loading rate; but in contrast, its hardness was somehow saturated. This behavior is likely interpreted as an obstructive effect of the high dislocation density of GaN/N_2, as displayed in Fig. 8b. Thus, the possibly dislocation mechanism scenarios, in such behavior, were the rapid collective movement of mobile dislocations [69] by increasing the loading rate. Accordingly, nano-cracks were generated and emerged at the surface's sample, which reduced the sample stiffness as revealed by the decline of the Young's modulus.

5. Conclusion

The present work reports on a comparative study of the nano-mechanical behavior and properties of GaN samples elaborated within H_2 and N_2 ambient, as carrier gases using MOCVD process. Nano-mechanical properties of two GaN thin films were determined by instrumented nanoindentation technique. To derive Young's modulus and hardness depth-dependent from only a single load–displacement curve, new method was proposed, as alternative to CSM technique. For this purpose, pure elastic unloading path was assumed and verified. Depending on the epitaxial growth mechanism of GaN (either 3D or 2D growth mode) dictated by the used carrier gas, its significant influence on the resulting nanomechanical behavior and physical features was revealed. The observed distinguish nanomechanical behavior and properties is mainly attributed to the distribution of pre-existing dislocations and to the dislocation density within the sample as a result of

Table 2
Maximum shear stress and plastic work calculated at different loading rates for both GaN samples.

Loading rates (mN/s)	GaN with H_2		GaN with N_2	
	Maximum shear stress τ_{max}(GPa)	Average of plastic work (10^{-12}J)	Maximum shear stress τ_{max}(GPa)	Average of plastic work (10^{-12}J)
0.3	17.3	368	16.2	265
0.5	20.6	356	16.2	266
1.0	24.2	345	16.3	264
3.0	28.4	327	16.5	266

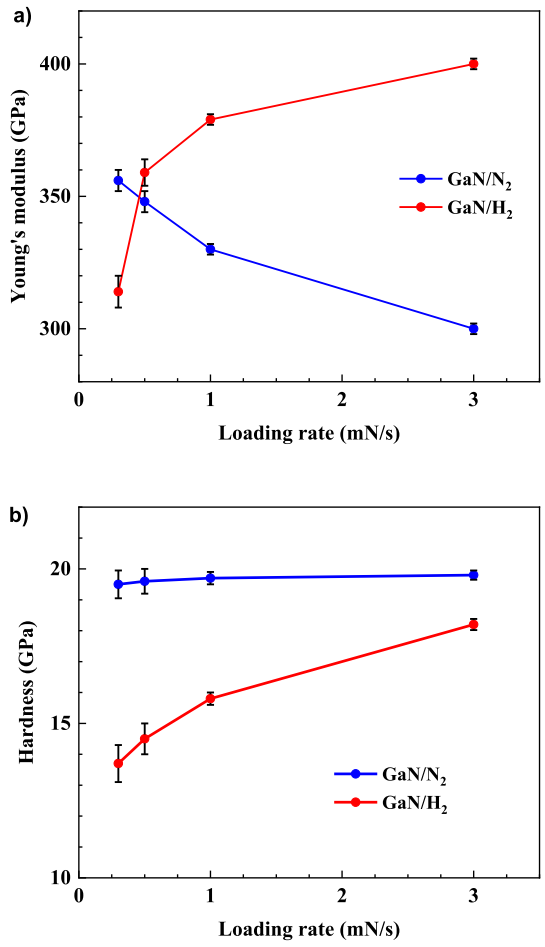

Fig. 12. Nanomechanical properties evolution as a function of the loading rate for GaN/H_2 and GaN/N_2 samples: a) Young's modulus; b) Hardness.

either the higher or the lower strain relaxation. Based on classical theory of dislocations, the occurrence of the pop-in event is attributed to homogeneous dislocation nucleation mechanism for the GaN/H_2 sample. However, for GaN/N_2 no such phenomenon was revealed; thus, the collective activation of pre-existing mobile dislocation is the most probable scenario. The fracture toughness coefficient K_{IC} was determined for GaN/N_2, where it was revealed cracks at Vickers microhardness imprint with a load of 1962 mN. For GaN/H_2, a pile-up was observed and no cracks was disclosed at sample's surface. In addition, the effect of loading rate on the nanomechanical behavior were shown for GaN/H_2, in contrary to the GaN/N_2 sample, where no effect was distinguished. Afterwards, these findings emphasis the decisive effect of elaboration conditions for GaN epilayers and permit a clear understanding of the close relationships between the resulting microstructure and the relevant changes in the nanomechanical behavior caused by specific dislocation mechanisms.

CRediT authorship contribution statement

Najla Boughrara: Methodology, Investigation, Writing – original draft, Writing – review & editing. **Zohra Benzarti:** Conceptualization, Methodology, Investigation, Supervision, Writing – original draft, Writing – review & editing. **Ali Khalfallah:** Conceptualization, Methodology, Investigation, Supervision, Writing – original draft, Writing – review & editing. **Manuel Evaristo:** Resources, Methodology. **Albano Cavaleiro:** Resources, Methodology.

Declaration of Competing Interest

The authors declare that they have no known competing financial interests or personal relationships that could have appeared to influence the work reported in this paper.

Acknowledgements

Dr. Ali Khalfallah gratefully acknowledge his support by FEDER funds through the program COMPETE – Programa Operacional Factores de Competitividade – and by national funds through FCT – Fundação para a Ciência e a Tecnologia, under the project UID/EMS/00285/2020. It was also supported by the project RDFORMING (reference PTDC/EMEEME/31243/2017), co-funded by Portuguese Foundation for Science and Technology, by FEDER, through the program Portugal-2020 (PT2020), and by POCI, with reference POCI-01-0145-FEDER-031243. Both supports are gratefully acknowledged.

Data availability

The raw/processed data required to reproduce these findings cannot be shared at this time as the data also form a part of an ongoing study.

References

[1] S. Nakamura, T. Mukai, M. Senoh, High-power gan p-n junction blue-light-emitting diodes, Jpn. J. Appl. Phys. 30 (1991) L1998–L2001, https://doi.org/10.1143/JJAP.30.L1998.
[2] Z. Benzarti, T. Sekrafi, Z. Bougrioua, A. Khalfallah, B. El Jani, Effect of SiN Treatment on Optical Properties of InxGa1−xN/GaN MQW Blue LEDs, J. Electron. Mater. 46 (7) (2017) 4312–4320, https://doi.org/10.1007/s11664-017-5383-2.
[3] F. Akyol, S. Krishnamoorthy, Y. Zhang, S. Rajan, GaN-based three-junction cascaded light-emitting diode with low-resistance InGaN tunnel junctions, Appl. Phys. Express. 8 (8) (2015) 082103, https://doi.org/10.7567/APEX.8.082103.
[4] Y. Li, Y. Jiang, J. Die, C. Wang, S. Yan, Z. Ma, H. Wu, L.u. Wang, H. Jia, W. Wang, H. Chen, Improvement of green InGaN-based LEDs efficiency using a novel quantum well structure, Chin. Phys. B. 26 (8) (2017) 087311, https://doi.org/10.1088/1674-1056/26/8/087311.
[5] Z. Benzarti, I. Halidou, O. Tottereau, T. Boufaden, B. El Jani, Silicon effect on GaN surface morphology, Microelectronics J. 33 (11) (2002) 995–998, https://doi.org/10.1016/S0026-2692(02)00066-6.
[6] S.J. Pearton, J.C. Zolper, R.J. Shul, F. Ren, GaN: Processing, defects, and devices, J. Appl. Phys. 86 (1) (1999) 1–78, https://doi.org/10.1063/1.371145.
[7] W.C. Oliver, G.M. Pharr, An improved technique for determining hardness and elastic modulus using load and displacement sensing indentation experiments, J. Mater. Res. 7 (6) (1992) 1564–1583.
[8] M.F. Doerner, W.D. Nix, A method for interpreting the data from depth-sensing indentation instruments, J. Mater. Res. 1 (4) (1986) 601–609, https://doi.org/10.1557/JMR.1986.0601.
[9] W.C. Oliver, G.M. Pharr, Measurement of hardness and elastic modulus by instrumented indentation: Advances in understanding and refinements to methodology, J. Mater. Res. 19 (1) (2004) 3–20, https://doi.org/10.1557/jmr.2004.19.1.3.
[10] C. Tromas, J.C. Girard, V. Audurier, J. Woirgard, Study of the low stress plasticity in single-crystal MgO by nanoindentation and atomic force microscopy, J. Mater. Sci. 34 (1999) 5337–5342, https://doi.org/10.1023/A:1004705206482.
[11] N. Gane, F.P. Bowden, Microdeformation of solids, J. Appl. Phys. 39 (3) (1968) 1432–1435, https://doi.org/10.1063/1.1656376.
[12] S.-R. Jian, G.-J. Chen, J.-C. Jang, Y.-S. Lai, Nanomechanical properties of AlN(1 0 3) thin films by nanoindentation, J. Alloys Compd. 494 (1-2) (2010) 219–222, https://doi.org/10.1016/j.jallcom.2009.11.166.
[13] Z. Benzarti, T. Sekrafi, A. Khalfallah, Z. Bougrioua, D. Vignaud, M. Evaristo, A. Cavaleiro, Growth temperature effect on physical and mechanical properties of nitrogen rich InN epilayers, J. Alloys Compd. 885 (2021) 160951, https://doi.org/10.1016/j.jallcom.2021.160951.
[14] R. Navamathavan, S.-J. Park, J.-H. Hahn, C.K. Choi, Nanoindentation "pop-in" phenomenon in epitaxial ZnO thin films on sapphire substrates, Mater. Charact. 59 (4) (2008) 359–364, https://doi.org/10.1016/j.matchar.2007.01.020.
[15] S.E. Grillo, M. Ducarroir, M. Nadal, E. Tourni, J.-P. Faurie, Nanoindentation of Si, GaP, GaAs and ZnSe single crystals, J. Phys. D. Appl. Phys. 36 (1) (2003) L5–L9, https://doi.org/10.1088/0022-3727/36/1/102.
[16] C.-H. Tsai, S.-R. Jian, J.-Y. Juang, Berkovich nanoindentation and deformation mechanisms in GaN thin films, Appl. Surf. Sci. 254 (7) (2008) 1997–2002, https://doi.org/10.1016/j.apsusc.2007.08.022.
[17] M. Fujikane, T. Yokogawa, S. Nagao, R. Nowak, Yield shear stress dependence on nanoindentation strain rate in bulk GaN crystal, Phys. Status Solidi Curr. Top. Solid State Phys. 8 (2011) 429–431, https://doi.org/10.1002/pssc.201000604.

[18] W. Li, S. Xu, Y. Zhang, R. Peng, J. Du, Y. Zhao, X. Fan, J. Zhang, H. Tao, X. Wang, Y. Hao, GaN quality evolution according to carrier gas for the nucleation layer and buffer layer, Opt. Mater. Express. 9 (4) (2019) 1945, https://doi.org/10.1364/OME.9.001945.

[19] O. Schön, B. Schineller, M. Heuken, R. Beccard, Comparison of hydrogen and nitrogen as carrier gas for MOVPE growth of GaN, J. Cryst. Growth. 189–190 (1998) 335–339, https://doi.org/10.1016/S0022-0248(98)00287-5.

[20] H. Amano, N. Sawaki, I. Akasaki, Y. Toyoda, Metalorganic vapor phase epitaxial growth of a high quality GaN film using an AlN buffer layer, Appl. Phys. Lett. 48 (5) (1986) 353–355, https://doi.org/10.1063/1.96549.

[21] Y.S. Cho, H. Hardtdegen, N. Kaluza, N. Thillosen, R. Steins, Z. Sofer, H. Lüth, Effect of carrier gas on GaN epilayer characteristics, Phys. Status Solidi. 3 (6) (2006) 1408–1411, https://doi.org/10.1002/pssc.200565121.

[22] I. Halidou, Z. Benzarti, H. Fitouri, W. Fathallah, B.E. Jani, GaN property evolution at all stages of MOVPE Si/N treatment growth, Phys. Status Solidi. 4 (1) (2007) 129–132, https://doi.org/10.1002/pssc.200673532.

[23] S.J. Vachhani, R.D. Doherty, S.R. Kalidindi, Effect of the continuous stiffness measurement on the mechanical properties extracted using spherical nanoindentation, Acta Mater. 61 (10) (2013) 3744–3751, https://doi.org/10.1016/j.actamat.2013.03.005.

[24] D.D. Koleske, M.E. Coltrin, K.C. Cross, C.C. Mitchell, A.A. Allerman, Understanding GaN nucleation layer evolution on sapphire, J. Cryst. Growth. 273 (1-2) (2004) 86–99, https://doi.org/10.1016/j.jcrysgro.2004.08.126.

[25] Y.S. Cho, H. Hardtdegen, N. Kaluza, R. Steins, G. Heidelberger, H. Lüth, The growth mechanism of GaN with different H2/N2 carrier gas ratios, J. Cryst. Growth. 307 (1) (2007) 6–13, https://doi.org/10.1016/j.jcrysgro.2007.05.058.

[26] J.E. Ayers, The measurement of threading dislocation densities in semiconductor crystals by X-ray diffraction, J. Cryst. Growth. 135 (1-2) (1994) 71–77, https://doi.org/10.1016/0022-0248(94)90727-7.

[27] X.J. Ning, F.R. Chien, P. Pirouz, J.W. Yang, M.A. Khan, Growth defects in GaN films on sapphire: The probable origin of threading dislocations, J. Mater. Res. 11 (3) (1996) 580–592, https://doi.org/10.1557/JMR.1996.0071.

[28] B.N. Sverdlov, G.A. Martin, H. Morkoç, D.J. Smith, Formation of threading defects in GaN wurtzite films grown on nonisomorphic substrates, Appl. Phys. Lett. 67 (14) (1995) 2063–2065, https://doi.org/10.1063/1.115079.

[29] T. Böttcher, S. Einfeldt, S. Figge, R. Chierchia, H. Heinke, D. Hommel, J.S. Speck, The role of high-temperature island coalescence in the development of stresses in GaN films, Appl. Phys. Lett. 78 (14) (2001) 1976–1978, https://doi.org/10.1063/1.1359780.

[30] T. Kozawa, T. Kachi, H. Kano, H. Nagase, N. Koide, K. Manabe, Thermal stress in GaN epitaxial layers grown on sapphire substrates, J. Appl. Phys. 77 (9) (1995) 4389–4392, https://doi.org/10.1063/1.359465.

[31] S. Ruvimov, Z. Liliental-Weber, T. Suski, J.W. Ager, J. Washburn, J. Krueger, C. Kisielowski, E.R. Weber, H. Amano, I. Akasaki, Effect of Si doping on the dislocation structure of GaN grown on the A-face of sapphire, Appl. Phys. Lett. 69 (7) (1996) 990–992, https://doi.org/10.1063/1.117105.

[32] P. Cantu, F. Wu, P. Waltereit, S. Keller, A.E. Romanov, S.P. DenBaars, J.S. Speck, Role of inclined threading dislocations in stress relaxation in mismatched layers, J. Appl. Phys. 97 (10) (2005) 103534, https://doi.org/10.1063/1.1897486.

[33] B. Monemar, Fundamental energy gap of gan from photoluminescence excitation spectra, Phys. Rev. B. 10 (2) (1974) 676–681, https://doi.org/10.1103/PhysRevB.10.676.

[34] W. Rieger, T. Metzger, H. Angerer, R. Dimitrov, O. Ambacher, M. Stutzmann, Influence of substrate-induced biaxial compressive stress on the optical properties of thin GaN films, Appl. Phys. Lett. 68 (7) (1996) 970–972, https://doi.org/10.1063/1.116115.

[35] D. Li, H. Chen, H.B. Yu, Y.J. Han, X.H. Zheng, Q. Huang, J.M. Zhou, Effects of carrier gas on the stress of a-plane GaN films grown on r-plane sapphire substrates by metalorganic chemical vapor deposition, J. Cryst. Growth. 263 (1-4) (2004) 76–79, https://doi.org/10.1016/j.jcrysgro.2003.11.060.

[36] S.-R. Jian, T.-H. Fang, D.-S. Chuu, Analysis of physical properties of III-nitride thin films by nanoindentation, J. Electron. Mater. 32 (6) (2003) 496–500, https://doi.org/10.1007/s11664-003-0132-0.

[37] K.L. Johnson, Contact Mechanics, Cambridge University Press (1985), https://doi.org/10.1017/CBO9781139171731.

[38] W.D. Nix, H. Gao, Indentation size effects in crystalline materials: A law for strain gradient plasticity, J. Mech. Phys. Solids. 46 (3) (1998) 411–425, https://doi.org/10.1016/S0022-5096(97)00086-0.

[39] W. Guo, On the Influence of Indenter Tip Geometry on the Indentification of Material Parameters in Indentation Testing, PhD Thesis. (2011).

[40] C.-H. Chien, S.-R. Jian, C.-T. Wang, J.-Y. Juang, J.C. Huang, Y.-S. Lai, Cross-sectional transmission electron microscopy observations on the Berkovich indentation-induced deformation microstructures in GaN thin films, J. Phys. D. Appl. Phys. 40 (13) (2007) 3985–3990, https://doi.org/10.1088/0022-3727/40/13/011.

[41] S.O. Kucheyev, J.E. Bradby, J.S. Williams, C. Jagadish, M.V. Swain, G. Li, Deformation behavior of ion-beam-modified GaN, Appl. Phys. Lett. 78 (2) (2001) 156–158, https://doi.org/10.1063/1.1335552.

[42] M. Fujikane, A. Inoue, T. Yokogawa, S. Nagao, R. Nowak, Mechanical properties characterization of c -plane (0001) and m -plane (10–10) GaN by nanoindentation examination, Phys. Status Solidi. 7 (7-8) (2010) 1798–1800, https://doi.org/10.1002/pssc.200983641.

[43] J. Huang, K. Xu, Y.M. Fan, M.T. Niu, X.H. Zeng, J.F. Wang, H. Yang, Nanoscale anisotropic plastic deformation in single crystal GaN, Nanoscale Res. Lett. 7 (2012) 2–5, https://doi.org/10.1186/1556-276X-7-150.

[44] A. Kailer, Y.G. Gogotsi, K.G. Nickel, Phase transformations of silicon caused by contact loading, J. Appl. Phys. 81 (7) (1997) 3057–3063, https://doi.org/10.1063/1.364340.

[45] J.E. Bradby, S.O. Kucheyev, J.S. Williams, J. Wong-Leung, M.V. Swain, P. Munroe, G. Li, M.R. Phillips, Indentation-induced damage in GaN epilayers, Appl. Phys. Lett. 80 (3) (2002) 383–385, https://doi.org/10.1063/1.1436280.

[46] S. Pathak, S.R. Kalidindi, Spherical nanoindentation stress-strain curves, Mater. Sci. Eng. R Reports. 91 (2015) 1–36, https://doi.org/10.1016/j.mser.2015.02.001.

[47] S.O. Kucheyev, J.E. Bradby, J.S. Williams, C. Jagadish, M.V. Swain, Mechanical deformation of single-crystal ZnO, Appl. Phys. Lett. 80 (6) (2002) 956–958, https://doi.org/10.1063/1.1448175.

[48] T.A. Michalske, J.E. Houston, Dislocation nucleation at nano-scale mechanical contacts, Acta Mater. 46 (2) (1998) 391–396, https://doi.org/10.1016/S1359-6454(97)00270-X.

[49] M.A. Lodes, A. Hartmaier, M. Göken, K. Durst, Influence of dislocation density on the pop-in behavior and indentation size effect in CaF2 single crystals: Experiments and molecular dynamics simulations, Acta Mater. 59 (11) (2011) 4264–4273, https://doi.org/10.1016/j.actamat.2011.03.050.

[50] T.-H. Ahn, C.-S. Oh, K. Lee, E.P. George, H.N. Han, Relationship between yield point phenomena and the nanoindentation pop-in behavior of steel, J. Mater. Res. 27 (1) (2012) 39–44, https://doi.org/10.1557/jmr.2011.208.

[51] C. Chen, H. Li, H. Xiang, X. Peng, Molecular dynamics simulation on B3-GaN thin films under nanoindentation, Nanomaterials. 8 (2018) 856, https://doi.org/10.3390/nano8100856.

[52] P. Feltham, R. Banerjee, Theory and application of microindentation in studies of glide and cracking in single crystals of elemental and compound semiconductors, J. Mater. Sci. 27 (6) (1992) 1626–1632, https://doi.org/10.1007/BF00542926.

[53] P.B. Hirsch, P. Pirouz, S.G. Roberts, P.D. Warren, Indentation plasticity and polarity of hardness on (111) faces of GaAs, Philos. Mag. B Phys. Condens. Matter; Stat. Mech. Electron. Opt. Magn. Prop. 52 (3) (1985) 759–784, https://doi.org/10.1080/13642818508240635.

[54] B.D. Beake, S. Goel, Incipient plasticity in tungsten during nanoindentation: Dependence on surface roughness, probe radius and crystal orientation, Int. J. Refract. Met. Hard Mater. 75 (2018) 63–69, https://doi.org/10.1016/j.ijrmhm.2018.03.020.

[55] L.i. Chang, L. Zhang, Mechanical behaviour characterisation of silicon and effect of loading rate on pop-in: A nanoindentation study under ultra-low loads, Mater. Sci. Eng. A. 506 (1-2) (2009) 125–129, https://doi.org/10.1016/j.msea.2008.11.021.

[56] A. Barnoush, M.T. Welsch, H. Vehoff, Correlation between dislocation density and pop-in phenomena in aluminum studied by nanoindentation and electron channeling contrast imaging, Scr. Mater. 63 (5) (2010) 465–468, https://doi.org/10.1016/j.scriptamat.2010.04.048.

[57] F. Pöhl, Pop-in behavior and elastic-to-plastic transition of polycrystalline pure iron during sharp nanoindentation, Sci. Rep. 9 (2019) 1–12, https://doi.org/10.1038/s41598-019-51644-5.

[58] D. Lorenz, A. Zeckzer, U. Hilpert, P. Grau, H. Johansen, H.S. Leipner, Pop-in effect as homogeneous nucleation of dislocations during nanoindentation, Phys. Rev. B - Condens. Matter Mater. Phys. 67 (2003), 172101, https://doi.org/10.1103/PhysRevB.67.172101.

[59] A. Barnoush, Correlation between dislocation density and nanomechanical response during nanoindentation, Acta Mater. 60 (3) (2012) 1268–1277, https://doi.org/10.1016/j.actamat.2011.11.034.

[60] B.R. Lawn, A.G. Evans, D.B. Marshall, Elastic/Plastic Indentation Damage in Ceramics: The Median/Radial Crack System, J. Am. Ceram. Soc. 63 (9-10) (1980) 574–581, https://doi.org/10.1111/j.1151-2916.1980.tb10768.x.

[61] A. Leyland, A. Matthews, On the significance of the H/E ratio in wear control: A nanocomposite coating approach to optimised tribological behaviour, Wear. 246 (1-2) (2000) 1–11, https://doi.org/10.1016/S0043-1648(00)00488-9.

[62] J. Musil, M. Jirout, Toughness of hard nanostructured ceramic thin films, Surf. Coatings Technol. 201 (9-11) (2007) 5148–5152, https://doi.org/10.1016/j.surfcoat.2006.07.020.

[63] M. Sebastiani, K.E. Johanns, E.G. Herbert, G.M. Pharr, Measurement of fracture toughness by nanoindentation methods: Recent advances and future challenges, Curr. Opin. Solid State Mater. Sci. 19 (6) (2015) 324–333, https://doi.org/10.1016/j.cossms.2015.04.003.

[64] M.D. Drory, J.W. Ager, T. Suski, I. Grzegory, S. Porowski, Hardness and fracture toughness of bulk single crystal gallium nitride, Appl. Phys. Lett. 69 (26) (1996) 4044–4046, https://doi.org/10.1063/1.117865.

[65] Y. Cheng, D. Cai, H. Wang, J. Wu, X. Liu, G. Zhang, T. Yu, Anisotropic Fracture Toughness of Bulk GaN, Phys. Status Solidi B. 255 (5) (2018) 1700515, https://doi.org/10.1002/pssb.201700515.

[66] I. Ratschinski, H.S. Leipner, F. Heyroth, W. Fränzel, O. Moutanabbir, R. Hammer, M. Jurisch, Indentation-induced dislocations and cracks in (0001) freestanding and epitaxial GaN, in: J. Phys. Conf. Ser., Institute of Physics Publishing, 2011: p. 12007. https://doi.org/10.1088/1742-6596/281/1/012007.

[67] X. Gao, Displacement burst and hydrogen effect during loading and holding in nanoindentation of an iron single crystal, Scr. Mater. 53 (11) (2005) 1315–1320, https://doi.org/10.1016/j.scriptamat.2005.06.042.

[68] M. Zamanzade, G. Hasemann, C. Motz, M. Krüger, A. Barnoush, Vacancy effects on the mechanical behavior of B2-FeAl intermetallics, Mater. Sci. Eng. A. 712 (2018) 88–96, https://doi.org/10.1016/j.msea.2017.11.054.

[69] J. Chen, L. Zhen, L. wei Fan, S. jie Yang, S. long Dai, W. zhu Shao, Portevin-Le Chatelier effect in Al-Zn-Mg-Cu-Zr aluminum alloy, Trans. Nonferrous Met. Soc. China (English Ed. 19 (2009) 1071–1075. https://doi.org/10.1016/S1003-6326(08)60408-2.